と考えられる.

これらの AIF 推定の誤差要因を回避するために，動脈を含むボクセルではなく脳組織の信号強度 - 時間曲線から AIF を推定する方法を著者らは提案している〔42〕.

5) デコンボリューション

脳組織の濃度 - 時間曲線 ($C_t(t)$) は下記のように表される〔1〕.

$$C_t(t)=\frac{\rho}{k_H} f R(t)\otimes C_a(t) \tag{3}$$

ここで，f は CBF，$R(t)$ は残余関数，$C_a(t)$ は AIF を表す．ρ は脳組織の密度であり，1.04 g/mL という値が使われている〔24〕．k_H は下記のように表される.

$$k_H=\frac{1-H_{LV}}{1-H_{SV}} \tag{4}$$

H_{SV} および H_{LV} は，それぞれ，毛細血管および太い血管におけるヘマトクリットを表す．H_{SV} は 0.25，H_{LV} は 0.45 という値が使われている〔24〕.

(3) 式を基に CBF，MTT，CBV を計算するには，まず，$fR(t)$ を求める．$R(t)$ は，造影剤が組織にデルタ関数の形で入力してから t 時間後に組織に残留している造影剤の割合（残留量÷組織に入った総量）を表している．$R(t)$ は $t=0$ にて 1 であり，時間が進むにつれて単調減少する関数である．したがって，$fR(0)$ は CBF に等しい．実際には，計算誤差を考慮して，$fR(t)$ の最大値を CBF とする〔37, 43〕．また，

$$\mathrm{MTT}=\int R(t)\,dt \tag{5}$$

という関係があるので，$fR(t)$ の積分値を $fR(t)$ の最大値 (f) で割ったものを MTT とすることもある〔37, 43〕.

CBV は次式を使って計算される〔1〕.

$$\mathrm{CBV}=\frac{k_H}{\rho}\frac{\int C_t(t)\,dt}{\int C_a(t)\,dt} \tag{6}$$

また，$fR(t)$ の積分値も CBV になる.

Central volume theorem〔44, 45〕により，

$$\mathrm{CBF}=\frac{\mathrm{CBV}}{\mathrm{MTT}} \tag{7}$$

という関係が成り立つので，3 つのうちいずれか 2 つのパラメータが決まれば，残りの 1 つは (7) 式により計算することができる.

$fR(t)$ を求めるためのさまざまな方法が提案されているが，現在もっとも信頼されて使用されている方法は特異値分解法 (SVD) である〔37, 43〕．次に，SVD 法における誤差要因を紹介する.

(3) 式では，AIF は，注目している組織の直前の動脈における濃度-時間曲線であると仮定されている．しかし，実際には，AIF は組織から離れた位置にある MCA や ICA にて決められることが多い．こうして決められた AIF と真の AIF の間には，造影剤到着時間のずれ（以下では delay と呼ぶ）が生じる可能性がある．加えて，AIF を決定した血管を造影剤が通過してから組織に到達するまでの間に bolus の形状が鈍る（以下では dispersion と呼ぶ）可能性もある．delay および dispersion は，SVD 法による CBF および MTT の定量値の誤差要因になることが示されている〔26, 46, 47〕．濃度 - 時間曲線の立ち上りの関数形を仮定して最小自乗法により各ボクセルの造影剤到着時間を推定し，実測の濃度 - 時間曲線全体を delay 時間の分だけシフトさせて，delay をなくす方法が提案されている〔26〕．また，(3) 式を数学的に修正して delay の影響を受けないようにした SVD 法も提案されている〔48, 49〕．ただし，これらの方法では dispersion の影響を除去することはできない．delay と dispersion の両方による誤差をなくすために，組織ごとに別々に，できるだけ近い動脈にて AIF を決める方法が提案されている〔28, 29〕．また，独立成分分析を用いてボクセルごとに AIF を推定する方法も提案されている〔50〕.

$C_t(t)$ および $C_a(t)$ の時間分解能が低いとデコンボリューションにおける計算誤差が大きくなることが示されている〔51〕．全脳をカバーできるような撮影条件では，時間分解能が低下するために CBF 定量値の誤差は大きくなると考えられる．計算誤差を小さくするためには，スライス枚数を制限して時間分解能を上げる必要があると考えられる〔51〕.

4. まとめ

DSC-MRI にて CBF を測定することの意義，定量方法，誤差要因および現在提案されている対処方法，さらに著者らの提案新法について概説した．DSC-MRI は検査の利便性という点では優

れていると考えられるが，複数の誤差要因があり現時点では未解決の問題も多い．提案されている新しい方法の有効性について今後さらに臨床データを使って検証を行う必要があると考えられる．

謝　辞

DSC-MRI に関してご教授をいただいた林拓也，山本明秀，飯田秀博（国立循環器病センター研究所・放射線医学部），佐藤博司（国立循環器病センター研究所・先進診断機器開発室），山田直明（国立循環器病センター・放射線診療部）各氏に深謝します．本研究の一部は新エネルギー・産業技術総合開発機構（NEDO）の助成，厚生労働科学研究費補助金「こころの健康科学研究」，厚生労働科学研究費補助金萌芽的先端医療技術推進研究により実施された．

文　献

〔1〕 Calamante F, Thomas DL, Pell GS et al: Measuring cerebral blood flow using magnetic resonance imaging techniques. J Cereb Blood Flow Metab **19**: 701-735, 1999

〔2〕 Schlaug G, Benfield A, Baird AE et al: The ischemic penumbra: operationally defined by diffusion and perfusion MRI. Neurology **53**: 1528-1537, 1999

〔3〕 Neumann-Haefelin T, Wittsack HJ, Wenserski F et al: Diffusion- and perfusion-weighted MRI. The DWI/PWI mismatch region in acute stroke. Stroke **30**: 1591-1597, 1999

〔4〕 Thijs VN, Adami A, Neumann-Haefelin T et al: Relationship between severity of MR perfusion deficit and DWI lesion evolution. Neurology **57**: 1205-1211, 2001

〔5〕 Calamante F, Gadian DG, Connelly A: Quantification of perfusion using bolus tracking magnetic resonance imaging in stroke: assumptions, limitations, and potential implications for clinical use. Stroke **33**: 1146-1151, 2002

〔6〕 Carroll TJ, Teneggi V, Jobin M et al: Absolute quantification of cerebral blood flow with magnetic resonance, reproducibility of the method, and comparison with H2(15)O positron emission tomography. J Cereb Blood Flow Metab **22**: 1149-1156, 2002

〔7〕 Ostergaard L: Cerebral perfusion imaging by bolus tracking. Top Magn Reson Imaging **15**: 3-9, 2004

〔8〕 山田直明：常磁性体の影響，造影剤．小塚隆弘，内藤博昭，原田貢士編：MRI の基礎と臨床．永井書店，大阪，1994, pp23-34

〔9〕 Boxerman JL, Hamberg LM, Rosen BR et al: MR contrast due to intravascular magnetic susceptibility perturbations. Magn Reson Med **34**: 555-566, 1995

〔10〕 Weisskoff RM, Zuo CS, Boxerman JL et al: Microscopic susceptibility variation and transverse relaxation: theory and experiment. Magn Reson Med **31**: 601-610, 1994

〔11〕 Simonsen CZ, Ostergaard L, Smith DF et al: Comparison of gradient- and spin-echo imaging: CBF, CBV, and MTT measurements by bolus tracking. J Magn Reson Imaging **12**: 411-416, 2000

〔12〕 Johnson KM, Tao JZ, Kennan RP et al: Intravascular susceptibility agent effects on tissue transverse relaxation rates in vivo. Magn Reson Med **44**: 909-914, 2000

〔13〕 Kiselev VG: On the theoretical basis of perfusion measurements by dynamic susceptibility contrast MRI. Magn Reson Med **46**: 1113-1122, 2001

〔14〕 Villringer A, Rosen BR, Belliveau JW et al: Dynamic imaging with lanthanide chelates in normal brain: contrast due to magnetic susceptibility effects. Magn Reson Med **6**: 164-174, 1988

〔15〕 Rosen BR, Belliveau JW, Chien D: Perfusion imaging by nuclear magnetic resonance. Magn Reson Q **5**: 263-281, 1989

〔16〕 Kennan RP, Zhong J, Gore JC: Intravascular susceptibility contrast mechanisms in tissues. Magn Reson Med **31**: 9-21, 1994

〔17〕 Kjolby BF, Ostergaard L, Kiselev VG: Theoretical model of intravascular paramagnetic tracers effect on tissue relaxation. Magn Reson Med **56**: 187-197, 2006

〔18〕 Enmi J, Hayashi T, Watabe H et al: Measurement of cerebral blood flow with dynamic susceptibility contrast MRI and comparison with O-15 positron emission tomography. International Congress Series **1265**: 150-158, 2004

〔19〕 Miyati T, Banno T, Mase M et al: Dual dynamic contrast-enhanced MR imaging. J Magn Reson Imaging **7**: 230-235, 1997

〔20〕 Vonken EP, van Osch MJ, Bakker CJ et al: Simultaneous quantitative cerebral perfusion and Gd-DTPA extravasation measurement with dual-echo dynamic susceptibility contrast MRI. Magn Reson Med **43**: 820-827, 2000

〔21〕 Donahue KM, Krouwer HG, Rand SD et al: Utility of simultaneously acquired gradient-echo and spin-echo cerebral blood volume and morphology maps in brain tumor patients. Magn Reson Med **43**: 845-853, 2000

〔22〕 Johnson G, Wetzel SG, Cha S et al: Measuring blood volume and vascular transfer constant from dynamic, T(2)*-weighted contrast-enhanced MRI. Magn Reson Med **51**: 961-968, 2004

〔23〕 Kim EJ, Kim DH, Lee SH et al: Simultaneous acquisition of perfusion and permeability from corrected relaxation rates with dynamic susceptibility contrast dual gradient echo. Magn Reson Imaging **22**: 307-314, 2004

〔24〕 Rempp KA, Brix G, Wenz F et al: Quantification of regional cerebral blood flow and volume with dynamic susceptibility contrast-enhanced MR imaging. Radiology **193**: 637-641, 1994

〔25〕 Carroll TJ, Rowley HA, Haughton VM: Automatic calculation of the arterial input function for cerebral perfusion imaging with MR imaging. Radiology **227**: 593-600, 2003

〔26〕 Ibaraki M, Shimosegawa E, Toyoshima H et al: Tracer delay correction of cerebral blood flow with dynamic susceptibility contrast-enhanced MRI. J Cereb Blood Flow Metab **25**: 378-390, 2005

〔27〕 Mlynash M, Eyngorn I, Bammer R et al: Automated method for generating the arterial input function on perfusion-weighted MR imaging: validation in patients with stroke. AJNR Am J Neuroradiol **26**: 1479-1486, 2005

〔28〕 Lorenz C, Benner T, Chen PJ et al: Automated perfusion-weighted MRI using localized arterial input functions.

J Magn Reson Imaging **24**: 1133-1139, 2006

〔29〕 Lorenz C, Benner T, Lopez CJ et al: Effect of using local arterial input functions on cerebral blood flow estimation. J Magn Reson Imaging **24**: 57-65, 2006

〔30〕 Murase K, Kikuchi K, Miki H et al: Determination of arterial input function using fuzzy clustering for quantification of cerebral blood flow with dynamic susceptibility contrast-enhanced MR imaging. J Magn Reson Imaging **13**: 797-806, 2001

〔31〕 Mouridsen K, Christensen S, Gyldensted L et al: Automatic selection of arterial input function using cluster analysis. Magn Reson Med **55**: 524-531, 2006

〔32〕 van Osch MJ, Vonken EJ, Viergever MA et al: Measuring the arterial input function with gradient echo sequences. Magn Reson Med **49**: 1067-1076, 2003

〔33〕 Akbudak E, Conturo TE: Arterial input functions from MR phase imaging. Magn Reson Med **36**: 809-815, 1996

〔34〕 Akbudak E, Norberg RE, Conturo TE: Contrast-agent phase effects: an experimental system for analysis of susceptibility, concentration, and bolus input function kinetics. Magn Reson Med **38**: 990-1002, 1997

〔35〕 Conturo TE, Akbudak E, Kotys MS et al: Arterial input functions for dynamic susceptibility contrast MRI: requirements and signal options. J Magn Reson Imaging **22**: 697-703, 2005

〔36〕 Vonken EJ, van Osch MJ, Bakker CJ et al: Measurement of cerebral perfusion with dual-echo multi-slice quantitative dynamic susceptibility contrast MRI. J Magn Reson Imaging **10**: 109-117, 1999

〔37〕 Ostergaard L, Sorensen AG, Kwong KK et al: High resolution measurement of cerebral blood flow using intravascular tracer bolus passages. Part II: Experimental comparison and preliminary results. Magn Reson Med **36**: 726-736, 1996

〔38〕 Ellinger R, Kremser C, Schocke MF et al: The impact of peak saturation of the arterial input function on quantitative evaluation of dynamic susceptibility contrast-enhanced MR studies. J Comput Assist Tomogr **24**: 942-948, 2000

〔39〕 Lin W, Celik A, Derdeyn C et al: Quantitative measurements of cerebral blood flow in patients with unilateral carotid artery occlusion: a PET and MR study. J Magn Reson Imaging **14**: 659-667, 2001

〔40〕 van Osch MJ, van der Grond J, Bakker CJ: Partial volume effects on arterial input functions: shape and amplitude distortions and their correction. J Magn Reson Imaging **22**: 704-709, 2005

〔41〕 van Osch MJ, Vonken EJ, Bakker CJ et al: Correcting partial volume artifacts of the arterial input function in quantitative cerebral perfusion MRI. Magn Reson Med **45**: 477-485, 2001

〔42〕 圓見純一郎，佐藤博司，山本明秀，他：DSC-MRIによる脳血流量測定における動脈入力関数推定方法に関する検討．第35回日本磁気共鳴医学会大会講演抄録集，2007, pp425

〔43〕 Ostergaard L, Weisskoff RM, Chesler DA et al: High resolution measurement of cerebral blood flow using intravascular tracer bolus passages. Part I: Mathematical approach and statistical analysis. Magn Reson Med **36**: 715-725, 1996

〔44〕 Stewart GN: Researches on the circulation time in organs and on the influences which affect it. Parts I-III. J Physiol **15**: 1, 1894

〔45〕 Meier P, Zierler KL: On the theory of the indicator-dilution method for measurement of blood flow and volume. J Appl Physiol **6**: 731-744, 1954

〔46〕 Calamante F, Gadian DG, Connelly A: Delay and dispersion effects in dynamic susceptibility contrast MRI: simulations using singular value decomposition. Magn Reson Med **44**: 466-473, 2000

〔47〕 Wu O, Ostergaard L, Koroshetz WJ et al: Effects of tracer arrival time on flow estimates in MR perfusion-weighted imaging. Magn Reson Med **50**: 856-864, 2003

〔48〕 Wu O, Ostergaard L, Weisskoff RM et al: Tracer arrival timing-insensitive technique for estimating flow in MR perfusion-weighted imaging using singular value decomposition with a block-circulant deconvolution matrix. Magn Reson Med **50**: 164-174, 2003

〔49〕 Smith MR, Lu H, Trochet S et al: Removing the effect of SVD algorithmic artifacts present in quantitative MR perfusion studies. Magn Reson Med **51**: 631-634, 2004

〔50〕 Calamante F, Morup M, Hansen LK: Defining a local arterial input function for perfusion MRI using independent component analysis. Magn Reson Med **52**: 789-797, 2004

〔51〕 Smith M, Salluzzi M, Frayne R: Adaptive SVD thresholding is shown to be more appropriate for partial brain scans (TR = 1 s) rather than full brain scans (TR = 2 s). the ISMRM 14th Annual Meeting, 2006, pp 1541

圓見純一郎（えんみ　じゅんいちろう）
2000年北海道大学大学院理学研究科化学第二専攻博士後期課程修了．同年千歳科学技術大学光科学部特別研究員．2001年㈱日本アレフ入社．同年（財）医療機器センター流動研究員（国立循環器病センター研究所放射線医学部へ派遣）．2004年国立循環器病センター流動研究員．2007年国立循環器病センター特任研究員．日本磁気共鳴医学会会員．

*　　*　　*

Stroke
JOURNAL OF THE AMERICAN HEART ASSOCIATION
American Stroke Association
A Division of American Heart Association

Delayed Postischemic Treatment With Fluvastatin Improved Cognitive Impairment After Stroke in Rats

Munehisa Shimamura, Naoyuki Sato, Masataka Sata, Hitomi Kurinami, Daisuke Takeuchi, Kouji Wakayama, Takuya Hayashi, Hidehiro Iida and Ryuichi Morishita

Stroke published online Nov 1, 2007;
DOI: 10.1161/STROKEAHA.107.485045
Stroke is published by the American Heart Association. 7272 Greenville Avenue, Dallas, TX 72514
 Print ISSN: 0039-2499. Online ISSN: 1524-4628

Delayed Postischemic Treatment With Fluvastatin Improved Cognitive Impairment After Stroke in Rats

Munehisa Shimamura, MD, PhD; Naoyuki Sato, MD, PhD; Masataka Sata, MD, PhD; Hitomi Kurinami, MD; Daisuke Takeuchi, MD; Kouji Wakayama, MD; Takuya Hayashi, MD, PhD; Hidehiro Iida, MD, PhD; Ryuichi Morishita, MD, PhD

Background and Purposes—Recent clinical evidences indicate that statins may have beneficial effects on the functional recovery after ischemic stroke. However, the effect of delayed postischemic treatment with statins is still unclear. In the present study, we evaluated the effects of fluvastatin in the chronic stage of cerebral infarction in a rat model.

Methods—Rats exposed to permanent middle cerebral artery occlusion were treated for 3 months with fluvastatin beginning from 7 days after stroke. MRI, behavioral analysis, and immunohistochemistry were performed.

Results—Two months of treatment with fluvastatin showed the significant recovery in spatial learning without the decrease in serum total cholesterol level and worsening of infarction. Microangiography showed a significant increase in capillary density in the peri-infarct region in fluvastatin-treated rats after 3 months of treatment. Consistently, BrdU/CD31-positive cells were significantly increased in fluvastatin-treated rats after 7 days of treatment. MAP1B-positive neurites were also increased in the peri-infarct region in fluvastatin-treated rats. In addition, rats treated with fluvastatin showed the reduction of superoxide anion after 7 days of treatment and the reduction of Aβ deposits in the thalamic nuclei after 3 months of treatment.

Conclusions—Thus, delayed postischemic administration of fluvastatin had beneficial effects on the recovery of cognitive function without affecting the infarction size after ischemic stroke. Pleiotropic effects of fluvastatin, such as angiogenesis, neuritogenesis, and inhibition of superoxide production and Aβ deposition, might be associated with a favorable outcome. **(*Stroke*. 2007;38:000-000.)**

Key Words: angiogenesis ■ cerebral infarct ■ microcirculation ■ statins

Despite conflicting data correlating cholesterol level with stroke, 2 early trials of HMG-CoA reductase inhibitors (statins) in patients after myocardial infarction patients showed a reduction in stroke risk as a secondary end point.[1] A meta-analysis of 9 statin intervention trials, which enrolled patients with coronary artery disease or those at high risk for coronary disease, demonstrated a 21% relative risk reduction for stroke after 5 years of treatment.[2] Another clinical evidence suggests that the commencement of statins within 4 weeks of a stroke results in a favorable 90-day outcome.[3] To clarify the effects of postischemic statin treatment, previous studies in which atorvastatin was started 1 day after stroke in rodents showed improvement of sensory motor deficit through induction of angiogenesis, neurogenesis, and synaptogenesis.[4,5] These pleiotropic effects of statins were shown to be the result of induction of vascular endothelial growth factor or brain-derived neurotrophic factor.[4] Additionally, the microvascular dysfunction in the posttreatment of stroke with recombinant human tissue-type plasminogen activator could be reduced by statins in rodent model.[6] However, the effect of delayed treatment with statins after ischemic stroke is still unknown. From this viewpoint, we investigated whether chronic statin treatment beginning 7 days after ischemic stroke had influences on neurological deficits and pathophysiology after the permanent middle cerebral artery occlusion (MCAo) model in rats.

Materials and Methods

Surgical Procedure

Male Wistar rats (270 to 300 grams; Charles River; Kanagawa, Japan) were used in this study. The right MCA was occluded by placement of poly-L-lysine–coated 4-0 nylon, as described previously.[7]

Protocol for Treatment and Behavioral Tests

Ten rats were only anesthetized (sham operation) and 32 rats were subjected to MCAo (day 1). Based on neuromuscular function on day 7, the rats were divided equally into saline-treated (n=16) or fluvastatin-treated (n=16) groups. Fluvastatin (5 mg/kg per day;

Received February 14, 2007; final revision received April 27, 2007; accepted May 30, 2007.

From Department of Advanced Clinical Science and Therapeutics (M.S., M.Sata, K.W.), Graduate School of Medicine, the University of Tokyo, Japan; Department of Clinical Gene Therapy (N.S., H.K., D.T., R.M.), Graduate School of Medicine, Osaka University, Japan; Department of Investigative Radiology (T.H., H.I.), National Cardiovascular Center, Research Institute, Japan.

Correspondence to Ryuichi Morishita, MD, PhD, Professor, Division of Clinical Gene Therapy, Graduate School of Medicine, Osaka University, 2-2 Yamada-oka, Suita 565-0871, Japan. E-mail morishit@cgt.med.osaka-u.ac.jp

Stroke **is available at http://stroke.ahajournals.org** **DOI: 10.1161/STROKEAHA.107.485045**

provided by Novartis Pharma) or saline was given by gavage from day 7 to 100. We chose the dose (5 mg/kg per day), because a previous report showed that this dose could effectively induce angiogenesis in ischemic limb.[8] On day 55, neuromuscular function and locomotor activity were evaluated in the surviving rats. Then, cognitive function was examined by Morris water maze from day 56 to 63, because the effects of neuronal regeneration could be detected not in the early stage but in the chronic stage of ischemic brain such as 49 to 53 days after the insult.[9] On day 96, MRI was performed. On day 100, microangiography was performed.

MRI

High-resolution T1-weighted fast spin echo sequence images (repetition time [TR]=1500 ms; echo time [TE]=10.3 ms; field of view [FOV]=4× 3 cm; matrix=256×192; slice thickness=1.5 mm; slice gap=0.5 mm; number of slices=16; number of excitation=10; total time=9.39 min) were obtained using a 3-T MRI scanner (Signa LX VAH/I; GE).

Sensory Motor Deficit and Locomotor Activity

Although there are various batteries for testing sensory motor deficit, we used a simple protocol.[10] For forelimb flexion, rats were held by the tail on a flat surface. Paralysis of the forelimbs was evaluated by the degree of left forelimb flexion. For torso twisting, rats were held by the tail on a flat surface. The degree of body rotation was checked. For lateral push, rats were pushed either left or right. Rats with right MCA occlusion showed weak or no resistance against a left push. For hind limb placement, one hind limb was removed from the surface. Rats with right MCA occlusion showed delayed or no replacement of the hind limb when it was removed from the surface.

Spontaneous activity was measured via the open field (0.69 m^2). We set the sensor, which also put beams on the field, at 30 cm above the field. The number of count, which is when the animal crosses the beam, was measured for 30 minutes.

Morris Water Maze Task

A cylindrical tank 1.5 m in diameter was filled with water (25°C), and a transparent platform 15 cm in diameter was placed at a fixed position in the center of 1 of the 4 quadrants (O'Hara & Co, Ltd). In the hidden platform trials, we performed the tests 4 times per day for 4 days. When the rat could not reach the platform, the latency was set at 60 sec. In the visible platform trials, the tests were performed 4 times per day for 4 days. The acquired data were averaged per day.

Evaluation of Capillary Density

Using a recently developed microangiographic technique,[11] capillary density and blood–brain barrier leakage were evaluated in the cerebral cortex after MCA occlusion. The area or length of vessels was analyzed with an angiogenesis image analyzer (version 1.0; Kurabo).

Immunohistochemical Study: Bromodeoxyuridine Labeling

To identify newly formed DNA, saline-treated (n=5) and fluvastatin-treated (n=5) rats received injections of bromodeoxyuridine (BrdU, 50 mg/kg; Sigma-Aldrich, Saint Louis, Mo) intraperitoneally starting on day 7 twice per day until day 13. Rats were euthanized on day 14. After the sections (8-μm thickness) was fixed in 10% formaldehyde/MeOH neutral buffer solution and blocked, they were incubated with mouse monoclonal anti-rat CD31 antibody (1:100; BD Biosciences; San Jose, Calif), goat polyclonal anti-doublecortin (anti-DCX; Santa Cruz) antibody (1:100; Santa Cruz, Calif), mouse monoclonal anti-NeuN antibody (1:1000; Chemicon, Temecula, Calif), or mouse monoclonal anti-MAP1B antibody (1:100; Sigma-Aldrich), followed by anti-mouse goat fluorescent antibody (1:1000 for NeuN and MAP1B, 1:400 for CD31, Alexa Flour 546, Molecular Probes; Eugene, Ore) or anti-goat donkey fluorescent antibody (1:1000 for DCX Alexa Fluor 546). For double immunostaining, these sections were fixed again and incubated in 2 N HCl at 37°C for 30 minutes. After blocking, they were incubated with rat monoclonal anti-BrdU antibody (1:200; Abcam, Cambridge, UK) followed by anti-rat goat fluorescent antibody (1:1000, Alexa Fluor 488). For immunohistochemical staining for Aβ, sections were pretreated for 30 minutes with hot (85°C) citrate buffer as described before.[12] Confocal images were acquired using an FV-300 (Olympus).

Table. Infarction Volume Calculated by MRI, Blood Pressure, and Serum Total Cholesterol

	Sham	MCAo+S	MCAo+F	*P*
Infarction volume in total rats (mm^3)	...	283.8±23.9	278.4±26.4	0.851
Type of infarction in Figure 1a (N of rats)				0.828
A	...	12	11	...
B	...	3	3	...
C	...	1	2	...
Infarction volume (mm^3) in type A rats	...	322.8±15.0	327.0±18.8	0.758
Systolic blood pressure (mm Hg) in type A rats				
Day 7	116.1±5.4	123.7±6.0	115.5±7.3	0.654
Day 56	146.5±4.7	148.3±2.7	136.1±5.2	0.132
Serum total cholesterol (mg/dl) in type A rats on day 56	85.9±5.6	75.3±3.5	73.5±2.7	0.949

Type A, low-intensity area seen in the dorsolateral and lateral portions of the neocortex and the entire caudate putamen; type B, low-intensity area seen in the dorsolateral and lateral portions of the neocortex and in part of the caudate putamen; type C, low-intensity area seen in part of the lateral neocortex and caudate putamen. MCAo+S, saline-treated rats after MCAo; MCAo+F, fluvastatin-treated rats after MCAo.

P, saline vs fluvastatin.

Quantitative Histological Analysis

To quantify the immunoreactivity for MAP1B and Aβ, the acquired image was analyzed by Image J (version 1.32; NIH).

Detection of Superoxide Anion in Brain Sections

Superoxide anion was detected on day 14 as described previously.[13] Because intact cortex showed red fluorescence, we calculated the ratio of fluorescence as follows: ratio of fluorescence=[fluorescence intensity in ischemic core or peri-infarct region]/[fluorescence intensity in intact region].

Statistical Analysis

All values are expressed as mean±SEM. To analyze the differences in the type of cerebral infarction, χ^2 test was performed. The latency, path length, and mean speed in Morris water maze and sensory motor deficits were analyzed by a 2-factor repeated-measure ANOVA. Post hoc analyses were performed, and the Scheffe test was applied to control the inflation in type I error. The value of the serum total cholesterol, the blood pressure, and the spontaneous activity was analyzed by Scheffe rules. The differences in the immunohistochemistry and the volume of infarction were assessed by Mann–Whitney *U* analyses. In all cases, $P<0.05$ was considered significant.

Results

Effects of Fluvastatin on Cognitive Impairment

To confirm the severity of cerebral infarction, all rats were examined by T1-weighted MRI after 89 days of treatment. Although the total volume of infarction calculated in T1-weighted images was not different between rats treated with

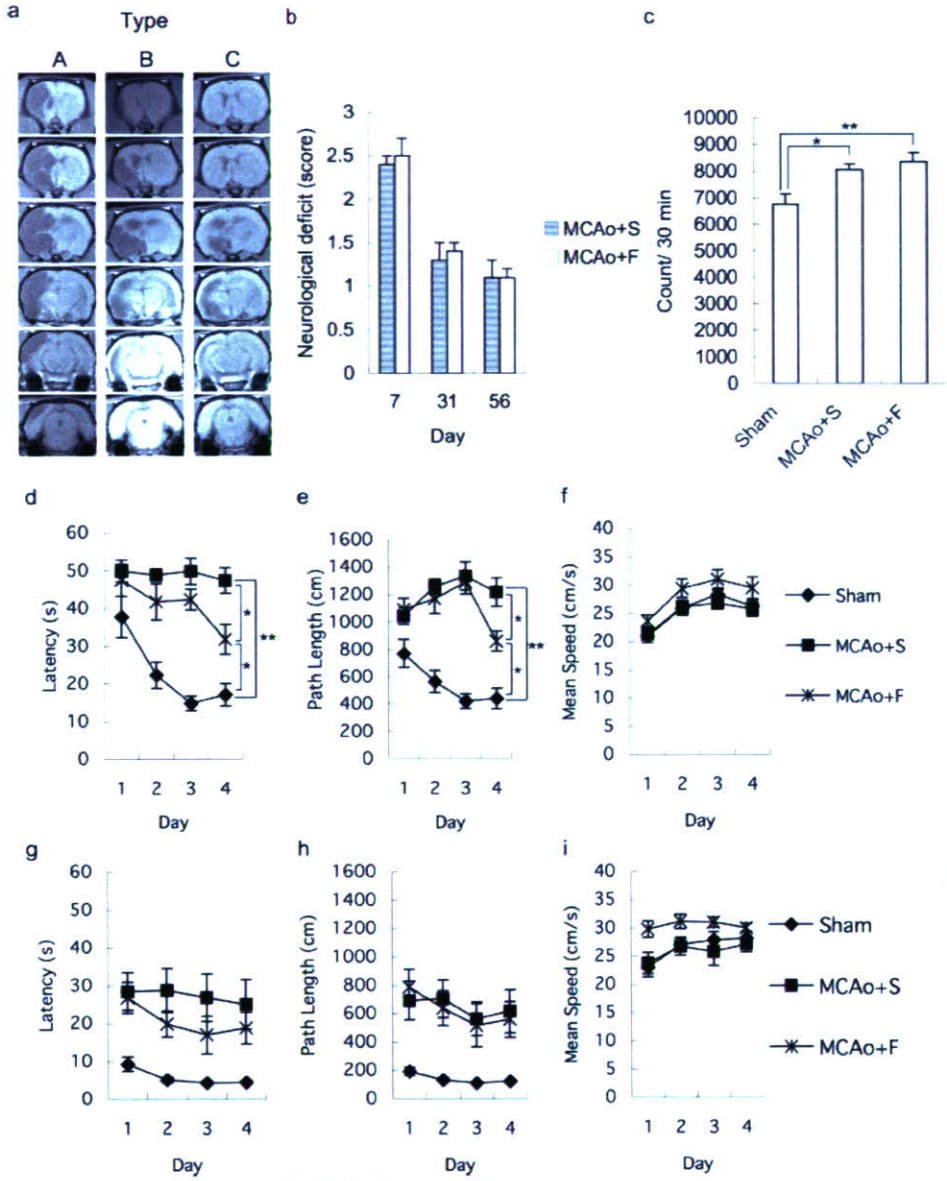

Figure 1. Typical T1-weighted image of coronal section of rat brain (a). The images were divided into 3 groups. Type A, low-intensity area seen in the dorsolateral and lateral portions of neocortex and the entire caudoputamen; type B, low-intensity area seen in the dorsolateral and lateral portions of neocortex and in part of the caudatoputamen; and type C, high-intensity area seen in part of the lateral neocortex and caudatoputamen. Sensory motor deficit (b). Spontaneous locomotor activity (c). Hidden platform test in Morris water maze. Each figure showed latency (d), path length (e), and mean speed (f). Days 1 to 4 indicate the trial day in the hidden platform test (56 to 59 days after middle cerebral artery occlusion). Visible platform test in Morris water maze. Each figure showed latency (g), path length (h), and mean speed (i). Days 1 to 4 indicate the day in the visible platform test (60 to 63 days after middle cerebral artery occlusion). MCAo+S indicates rats treated with saline after middle cerebral artery occlusion; MCAo+F, rats treated with fluvastatin after middle cerebral artery occlusion.

saline and fluvastatin (Table), the pattern of cerebral infarction was divided into 3 groups: type A, low-intensity area seen in the dorsolateral and lateral portions of the neocortex and the entire caudate putamen; type B, low-intensity area seen in the dorsolateral and lateral portions of the neocortex and in part of the caudate putamen; type C, low-intensity area seen in part of the lateral neocortex and caudate putamen (Figure 1a). In type C, most of the lateral neocortex was intact. To exclude the influence of the pattern of cerebral infarction on cognitive function, we focused on type A rats in the present study. The volume of cerebral infarction in type A rats was not different between the groups (Table). Blood pressure and serum total cholesterol also showed no difference among the groups (Table).

Sensory motor deficit had spontaneously recovered to some extent by 8 weeks in both groups, and there was no difference (Figure 1b). Locomotor activity in rats subjected to MCAo was increased as compared with that in sham-operated rats, as described before,[14] but there was no significant difference between fluvastatin-treated and saline-treated rats (Figure 1c). In Morris water maze (Figure 1d-i), which examines spatial learning, there were significant differences

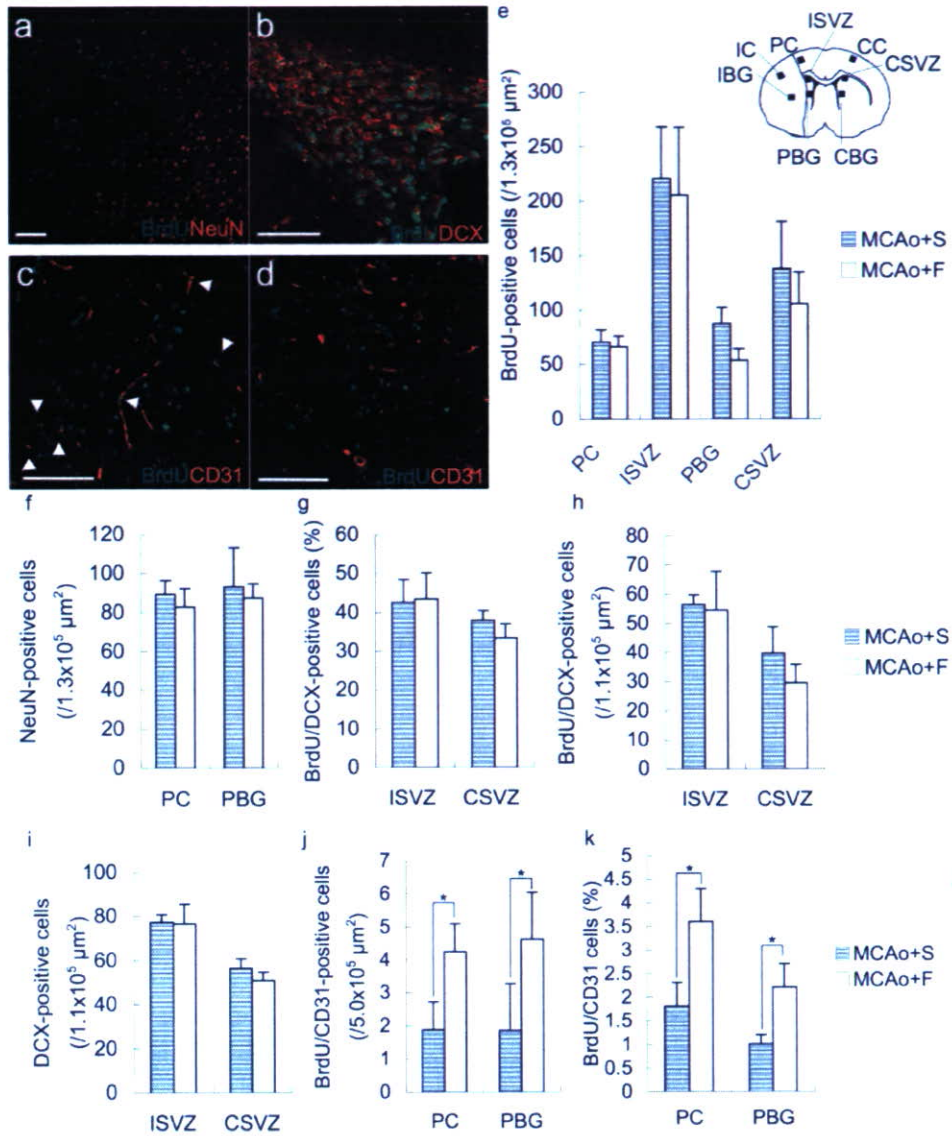

Figure 2. Representative images of immunohistochemical staining on day 14. Rats treated with fluvastatin (a through c), rats treated with saline (d). Although BrdU-positive cells were observed in the peri-infarct cortex (a), peri-infarct basal ganglia, and subventricular zone, these cells did not express NeuN (a), but expressed DCX in the subventricular zone (b). Fluvastatin-treated rats showed some BrdU/CD31-positive cells (arrows, c), although most BrdU-positive cells were negative for CD31 in saline-treated rats (d). The number of BrdU-positive cells (e), NeuN-positive cells (f), BrdU/DCX-positive cells (h), DCX-positive cells (i), and BrdU/CD31-positive cells (j); the percentage of BrdU/DCX-positive cells (g) or BrdU/CD31 cells (k) in total BrdU-positive cells. PC indicates peri-infarct cortex; PBG, peri-infarct basal ganglia; IC, infarcted cortex; IBG, ischemic basal ganglia; ISVZ, subventricular zone on infarcted side; CC, contralateral cortex, CSVZ, subventricular zone on contralateral side; CBG, contralateral basal ganglia (n=5 in each group, $^*P<0.05$, bar=100 μm).

in the latency and path length in hidden platform test among the groups (supplemental Table I, available online at http://stroke.ahajournals.org). A significant difference was observed on day 4 between fluvastatin-treated and saline-treated rats (supplemental Table I). Also, there was a significant difference between sham and saline-treated rats (supplemental Table I). There was no significant difference both in swimming speed and visible platform test, which excluded the possible influence of visual loss, sensory motor deficit, and motivation on the results.[15] These data suggest that impaired spatial learning was improved by fluvastatin.

Histological Changes by Fluvastatin

Next, we studied whether fluvastatin had some influences on the histology. Initially, we focused on neurogenesis and angiogenesis. To examine neurogenesis, we measured BrdU-incorporated cells after injecting BrdU from day 7 to day 13. Although BrdU-positive cells were observed in the subventricular zone and peri-infarct region (Figure 2a to 2d), the total number did not differ between the groups (Figure 2e). Similarly, the density of NeuN-positive cells, as a marker of adult neurons, also did not differ between the groups (Figure 2f), whereas there were no BrdU/NeuN-positive cells in the

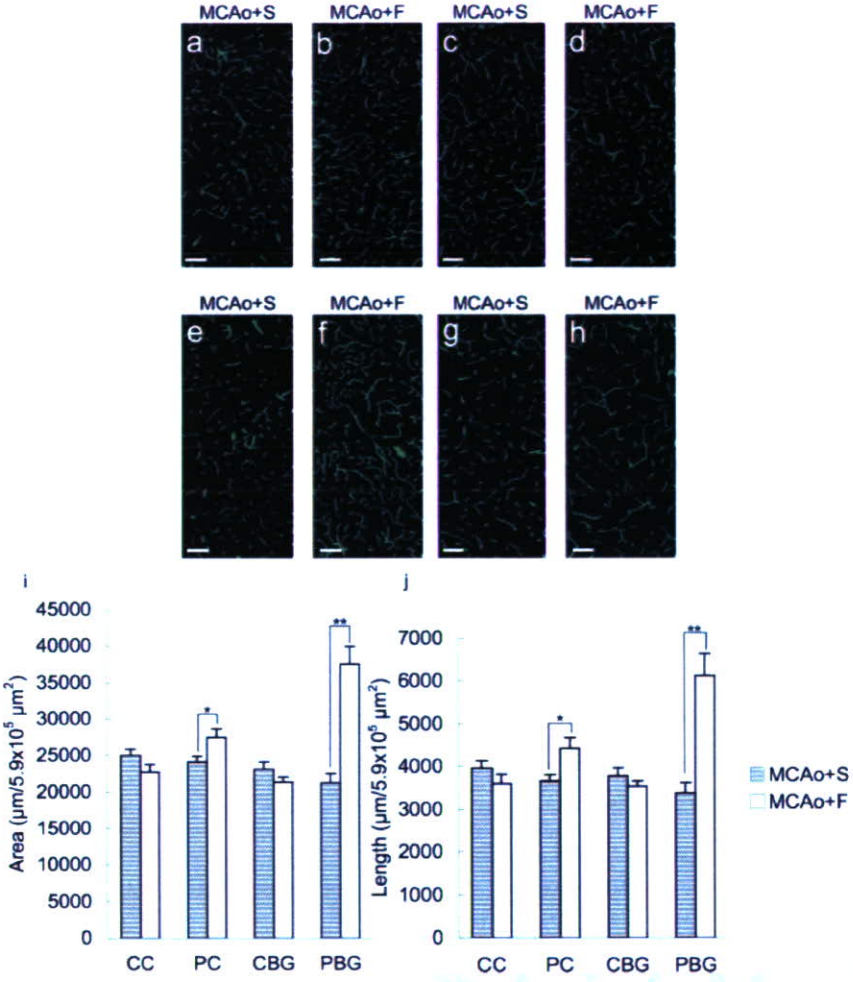

Figure 3. Microangiographic images using albumin-fluorescence isothiocyanate on day 100: (a and b) peri-infarct cortex; (c and d) contralateral cortex; (e and f) peri-infarct basal ganglia; (g and h) contralateral basal ganglia (bar=100 μm). Quantitative analysis (i and j) of microangiography. Rats treated with fluvastatin showed increased microvessels in the peri-infarct region (n=4 in each group, $^{*}P<0.05$, $^{**}P<0.01$).

peri-infarct cortex and subventricular zone (Figure 2a). Although some BrdU-positive cells expressing DCX, a marker for migrating neuroblasts, could be detected in subventricular zone (Figure 2b), the percentage in total BrdU-positive cells (Figure 2g) and the number (Figure 2h) did not differ between the groups. Also, the number of DCX-positive cells was same in the both groups (Figure 2i). There were no BrdU-positive cells expressing DCX in the cerebral cortex. Unexpectedly, these data suggest that neurogenesis was not enhanced by fluvastatin.

Thus, we further examined whether angiogenesis was affected by fluvastatin. In the peri-infarct cortex and basal ganglia, BrdU-positive cells that were positive for CD31 as a marker of endothelial cells could be detected (Figure 2c,2d). The number of BrdU/CD31-double-positive cells was significantly increased in fluvastatin-treated rats (Figure 2j). The percentage of BrdU/CD31-double-positive cells in total BrdU-positive cells was also increased in fluvastatin-treated rats (Figure 2k). Consistently, microangiography using FITC-conjugated albumin[11] also showed that microvessels were significantly increased in fluvastatin-treated rats only in the peri-infarct cortex and basal ganglia, without destruction of the blood–brain (Figure 3a to 3h). Quantitative analysis showed that the length and area of microvessels were also increased in the peri-infarct region, but not in the contralateral cortex and contralateral basal ganglia, in rats treated with fluvastatin, at 3 months after stroke (Figure 3i,j).

Because recent reports showed that neurite outgrowth was observed in the peri-infarct region from 7 to 14 days after cerebral infarction,[16,17] we next examined the effect of fluvastatin on neurite outgrowth. Immunohistochemical staining showed that treatment with fluvastatin significantly increased the immunoreactivity of MAP1B, a marker of neurite outgrowth, in neurites[16,18] (Figure 4), although the number of MAP1B-positive cells was the same in both groups. These data implied that the fluvastatin might promote angiogenesis, resulting in improvement of the microcirculation, and neurite outgrowth.

One possible explanation for the enhanced angiogenesis and neurite outgrowth is a decrease in oxidative stress by fluvastatin. To assess oxidative stress, we evaluated superoxide production using dihydroethidium staining (Figure 5a to 5e). Superoxide anion was increased in the ischemic core as compared with the contralateral region at 2 weeks after MCA occlusion (Figure 5a,5c). However, rats treated with fluvastatin showed a significant reduction in superoxide anion especially in the ischemic core region, but not in the peri-infarct cortex and basal ganglia (Figure 5b,5d,5e).

Finally, we examined Aβ deposition in the thalamic nuclei, because previous reports showed that Aβ deposits in the

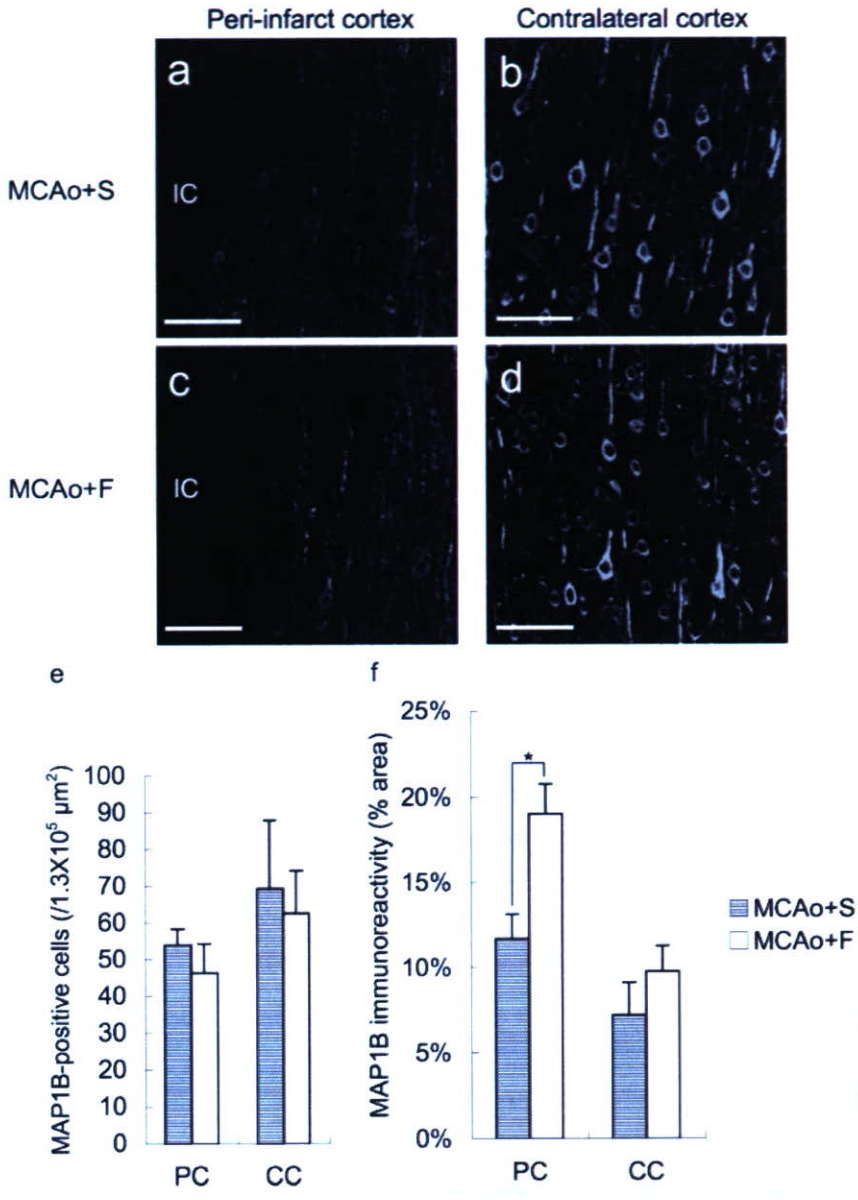

Figure 4. Typical images of immunohistochemical staining for MAP1B in peri-infarct cortex (a and c) and contralateral cortex (b and d) on day 14 (bar=100 μm). Although the number of MAP1B-positive cells was the same in both groups (e), immunoreactivity was higher in the peri-infarct region in fluvastatin-treated rats (f) (n=4 in each group, $^*P<0.05$).

thalamic nuclei persisted as long as 9 months after focal cerebral ischemia.[12] Although immunohistochemical staining showed marked deposition of Aβ in the ventrolateral and ventromedial thalamic nuclei at 3 months after stroke, the area of Aβ deposits was significantly decreased in fluvastatin-treated rats (Figure 5f to 5h). In other regions, such as cortex or basal ganglia, there was no Aβ deposits in both groups as reported before.[12]

Discussion

Although several laboratories have shown that long-term pretreatment with a statin reduces infarct size in rodents,[19] no articles have reported the effects of delayed postischemic treatment with statins. The present study demonstrated that statin treatment beginning 7 days after ischemic stroke resulted in significant improvement of spatial learning at 8 weeks after stroke, without any change in the plasma cholesterol level and infarct size.

Fluvastatin-treated rats showed a significant increase of MAP1B in neurites in the peri-infarct region. Considering that MAP1B is especially prominent in extending neurites[20] and related to functional recovery after ischemic stroke,[17] one of the possible effects of fluvastatin is to enhance neurite outgrowth, "neuritogenesis," in the early stage of treatment. This speculation might be supported by the recent study demonstrating that neurite outgrowth is accelerated by pravastatin via inhibiting the activity of geranylgeranylated proteins such as RhoA.[21]

As BrdU/CD31-positive cells were increased 14 days after MCAo and microvessels were also increased in the peri-infarct region 100 days after MCAo, fluvastatin enhanced angiogenesis and resulted in improvement of microcirculation in the peri-infarct region. Although the relationship between the improved microcirculation and behavior is still unclear, a recent report demonstrated that the restoration of perfusion by collateral growth and new capillaries in the

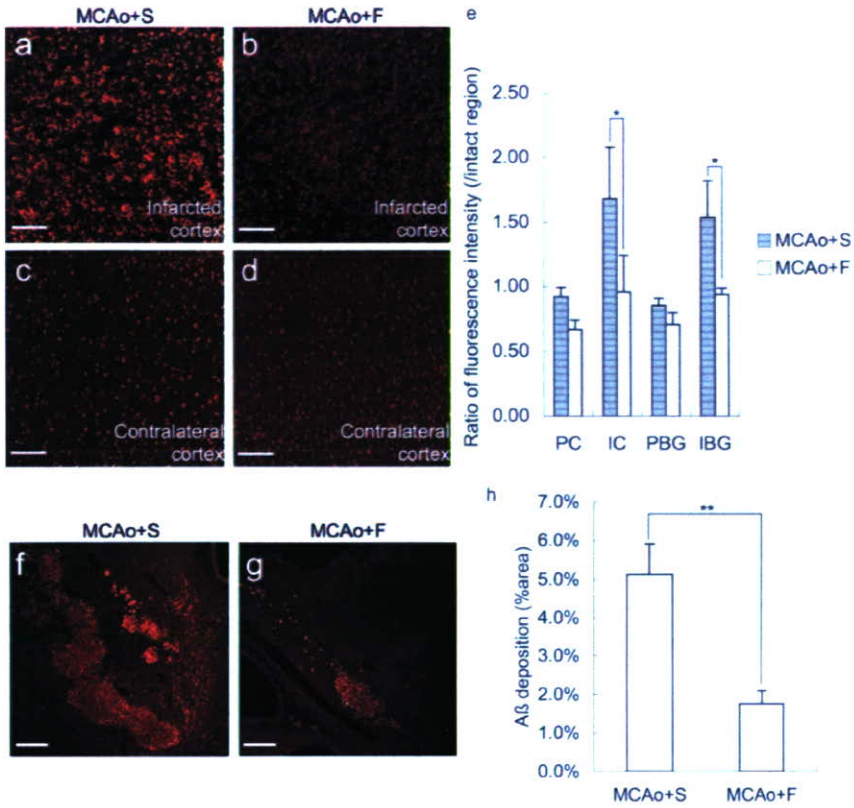

Figure 5. a through e, Superoxide anion detected by dihydroethidium staining on day 14. Red spots show the existence of superoxide anion. Fluorescence intensity was higher in the infarcted cortex (a) compared with the contralateral cortex (c). Fluvastatin-treated rats showed decreased fluorescence intensity in the infarcted cortex (b), although there was no difference in the peri-infarct cortex and basal ganglia (e) (n=4 in each group, $^{*}P<0.05$, bar=100 μm). Deposition of Aβ in thalamus on day 100 after middle cerebral artery occlusion. Although deposition of Aβ was observed in the thalamic nuclei (f and g), there was no deposition in other regions such as the cortex and basal ganglia. Quantitative analysis showed decreased Aβ deposition in fluvastatin-treated rats (h) (n=6 in each group, $^{**}P<0.01$, bar=200 μm).

ischemic border zone around a cortical infarct supported long-term functional recovery in rats.[22] Additionally, others reported that some patients who received tissue plasminogen activator therapy with no immediate clinical improvement despite early recanalization showed delayed clinical improvement.[23] From these viewpoints, it is likely that the improvement of microcirculation is an important factor for the functional recovery.

Of importance, fluvastatin reduced deposition of Aβ in the ventrolateral–ventromedial thalamic nuclei in the chronic stage of ischemic stroke, although rats subjected to focal cerebral ischemia develop deposition of Aβ in the ventroposterior lateral and ventroposterior medial nuclei for as long as 9 months.[12] This might be similar with precious reports showing that statins reduced the production of Aβ in Alzheimer disease.[24] The mechanism of the reduction of Aβ by fluvastatin should be further investigated.

Thus, the rats treated with fluvastatin showed enhancement of angiogenesis and neurite outgrowth in the peri-infarct cortex and reduced deposition of Aβ in the ventrolateral–ventromedial thalamic nuclei. Because those regions are important sites for spatial learning,[25,26] we speculate that the enhancement of functional recovery by fluvastatin might be dependent on those regions.

The other histological difference was the reduction of superoxide anion in the ischemic core in fluvastatin-treated rats. Because cerebral blood flow in the ischemic cortex remained to be reduced for 48 hours and restored to some extent 9 days after permanent MCAo,[27] we speculate that fluvastatin could reach the ischemic core and show the antioxidative effects. On the contrary, in the peri-infarct region, superoxide anion was not detected even in the control group and no effect of fluvastatin might be observed. This effect of statin is similar with the previous report showing that cerivastatin prevented the production of superoxide anion in the cerebral parenchyma in stroke-prone spontaneously hypertensive rats.[28] Also, fluvastatin is reported to possess antioxidative properties in other cells.[29,30]

The association of neurogenesis is also the center of interest, because previous reports showed an increase in neurogenesis after atorvastatin treatment beginning at 1 day after stroke.[5] However, we speculate that neurogenesis might not have contributed to the favorable outcome in the present study, because the volume of infarction was not decreased by fluvastatin, and the density of mature neurons (NeuN-positive cells) and proliferative immature neurons (BrdU/DCX-positive cells) was the same in both groups. From the viewpoints, the timing of treatment seems important for the enhancement of neurogenesis and the beginning of statin 7 days after MCAo might be too late to enhance neurogenesis.

The limitation of the present study is that there is no data demonstrating that fluvastatin crossed over the blood–brain barrier and acted on neurons directly. Blood–brain barrier permeability differs among statins and correlates in part with their respective lipophilicity.[31] Considering that pretreatment with pravastatin and rosuvastatin, whose lipophilicity is 0.84 and 0.33, respectively, shows significant effects on reducing infarction volume,[31] fluvastatin, whose lipophilicity is 1.27, might penetrate blood–brain barrier and have some direct effects on neurons. Otherwise, fluvastatin could penetrate the brain because of the disruption of blood–brain barrier after MCAo. One of other limitations in the present study is no

examination of the characteristics of BrdU positive-cells other than CD31, DCX, or NeuN. In addition, how these histological changes in fluvastatin-treated rats were mechanistically linked to improved outcome was not clarified. Further study is necessary to clarify these points.

Summary

Overall, delayed postischemic chronic fluvastatin treatment showed beneficial effects on the recovery of cognitive impairment after stroke by enhancement of neuritogenesis and of angiogenesis and a decrease in Aβ deposition and superoxide anion production. Further studies might show potential clinical utility to treat cognitive impairment in patients with ischemic stroke.

Acknowledgments

The authors thank Dr Masatsugu Horiuchi and Dr Masaru Iwai for their helpful advice on superoxide detection by dihydroethidium staining, and Dr Hiroshi Sato for assistance with MRI.

Sources of Funding

This work was partially supported by a Grant-in-Aid from the Organization for Pharmaceutical Safety and Research, a Grant-in-Aid from The Ministry of Public Health and Welfare, a Grant-in-Aid from Japan Promotion of Science, and a Grant-in-Aid from the Ministry of Education, Culture, Sports, Science, and Technology, of the Japanese Government.

Disclosures

Fluvastatin was donated from Novartis Pharma. Masataka Sata received Honoraria payment (modest) from Novartis Pharma. Ryuichi Morishita received honoraria payment (modest) and has an advisory board relationship to Novartis Pharma.

References

1. Sacks FM, Pfeffer MA, Moye LA, Rouleau JL, Rutherford JD, Cole TG, Brown L, Warnica JW, Arnold JM, Wun CC, Davis BR, Braunwald E. The effect of pravastatin on coronary events after myocardial infarction in patients with average cholesterol levels: cholesterol and recurrent events trial investigators. *N Engl J Med*. 1996;335:1001–1009.
2. Amarenco P, Tonkin AM. Statins for stroke prevention: disappointment and hope. *Circulation*. 2004;109:III44–49.
3. Moonis M, Kane K, Schwiderski U, Sandage BW, Fisher M. HMG-CoA reductase inhibitors improve acute ischemic stroke outcome. *Stroke*. 2005;36:1298–1300.
4. Chen J, Zhang C, Jiang H, Li Y, Zhang L, Robin A, Katakowski M, Lu M, Chopp M. Atorvastatin induction of VEGF and BDNF promotes brain plasticity after stroke in mice. *J Cereb Blood Flow Metab*. 2005;25:281–290.
5. Chen J, Zhang ZG, Li Y, Wang Y, Wang L, Jiang H, Zhang C, Lu M, Katakowski M, Feldkamp CS, Chopp M. Statins induce angiogenesis, neurogenesis, and synaptogenesis after stroke. *Ann Neurol*. 2003;53:743–751.
6. Zhang L, Zhang ZG, Ding GL, Jiang Q, Liu X, Meng H, Hozeska A, Zhang C, Li L, Morris D, Zhang RL, Lu M, Chopp M. Multitargeted effects of statin-enhanced thrombolytic therapy for stroke with recombinant human tissue-type plasminogen activator in the rat. *Circulation*. 2005;112:3486–3494.
7. Belayev L, Alonso OF, Busto R, Zhao W, Ginsberg MD. Middle cerebral artery occlusion in the rat by intraluminal suture: neurological and pathological evaluation of an improved model. *Stroke*. 1996;27:1616–1623.
8. Sata M, Nishimatsu H, Osuga J, Tanaka K, Ishizaka N, Ishibashi S, Hirata Y, Nagai R. Statins augment collateral growth in response to ischemia but they do not promote cancer and atherosclerosis. *Hypertension*. 2004;43:1214–1220.
9. Nakatomi H, Kuriu T, Okabe S, Yamamoto S, Hatano O, Kawahara N, Tamura A, Kirino T, Nakafuku M. Regeneration of hippocampal pyramidal neurons after ischemic brain injury by recruitment of endogenous neural progenitors. *Cell*. 2002;110:429–441.
10. Petullo D, Masonic K, Lincoln C, Wibberley L, Teliska M, Yao DL. Model development and behavioral assessment of focal cerebral ischemia in rats. *Life Sci*. 1999;64:1099–1108.
11. Cavaglia M, Dombrowski SM, Drazba J, Vasanji A, Bokesch PM, Janigro D. Regional variation in brain capillary density and vascular response to ischemia. *Brain Res*. 2001;910:81–93.
12. van Groen T, Puurunen K, Maki HM, Sivenius J, Jolkkonen J. Transformation of diffuse beta-amyloid precursor protein and beta-amyloid deposits to plaques in the thalamus after transient occlusion of the middle cerebral artery in rats. *Stroke*. 2005;36:1551–1556.
13. Iwai M, Liu HW, Chen R, Ide A, Okamoto S, Hata R, Sakanaka M, Shiuchi T, Horiuchi M. Possible inhibition of focal cerebral ischemia by angiotensin II type 2 receptor stimulation. *Circulation*. 2004;110:843–848.
14. Robinson RG. Differential behavioral and biochemical effects of right and left hemispheric cerebral infarction in the rat. *Science*. 1979;205:707–710.
15. DeVries AC, Nelson RJ, Traystman RJ, Hurn PD. Cognitive and behavioral assessment in experimental stroke research: Will it prove useful? *Neurosci Biobehav Rev*. 2001;25:325–342.
16. Badan I, Platt D, Kessler C, Popa-Wagner A. Temporal dynamics of degenerative and regenerative events associated with cerebral ischemia in aged rats. *Gerontology*. 2003;49:356–365.
17. Badan I, Dinca I, Buchhold B, Suofu Y, Walker L, Gratz M, Platt D, Kessler CH, Popa-Wagner A. Accelerated accumulation of n- and c-terminal beta app fragments and delayed recovery of microtubule-associated protein 1b expression following stroke in aged rats. *Eur J Neurosci*. 2004;19:2270–2280.
18. Schabitz WR, Berger C, Kollmar R, Seitz M, Tanay E, Kiessling M, Schwab S, Sommer C. Effect of brain-derived neurotrophic factor treatment and forced arm use on functional motor recovery after small cortical ischemia. *Stroke*. 2004;35:992–997.
19. Endres M, Laufs U, Liao JK, Moskowitz MA. Targeting enos for stroke protection. *Trends Neurosci*. 2004;27:283–289.
20. Gonzalez-Billault C, Avila J, Caceres A. Evidence for the role of map1b in axon formation. *Mol Biol Cell*. 2001;12:2087–2098.
21. Pooler AM, Xi SC, Wurtman RJ. The 3-hydroxy-3-methylglutaryl co-enzyme a reductase inhibitor pravastatin enhances neurite outgrowth in hippocampal neurons. *J Neurochem*. 2006;97:716–723.
22. Wei L, Erinjeri JP, Rovainen CM, Woolsey TA. Collateral growth and angiogenesis around cortical stroke. *Stroke*. 2001;32:2179–2184.
23. Alexandrov AV, Hall CE, Labiche LA, Wojner AW, Grotta JC. Ischemic stunning of the brain: Early recanalization without immediate clinical improvement in acute ischemic stroke. *Stroke*. 2004;35:449–452.
24. Fassbender K, Simons M, Bergmann C, Stroick M, Lutjohann D, Keller P, Runz H, Kuhl S, Bertsch T, von Bergmann K, Hennerici M, Beyreuther K, Hartmann T. Simvastatin strongly reduces levels of Alzheimer's disease beta -amyloid peptides Abeta 42 and Abeta 40 in vitro and in vivo. *Proc Natl Acad Sci U S A*. 2001;98:5856–5861.
25. Casu MA, Wong TP, De Koninck Y, Ribeiro-da-Silva A, Cuello AC. Aging causes a preferential loss of cholinergic innervation of characterized neocortical pyramidal neurons. *Cereb Cortex*. 2002;12:329–337.
26. Jeljeli M, Strazielle C, Caston J, Lalonde R. Effects of ventrolateral-ventromedial thalamic lesions on motor coordination and spatial orientation in rats. *Neurosci Res*. 2003;47:309–316.
27. Rudin M, Baumann D, Ekatodramis D, Stirnimann R, McAllister KH, Sauter A. MRI analysis of the changes in apparent water diffusion coefficient, t(2) relaxation time, and cerebral blood flow and volume in the temporal evolution of cerebral infarction following permanent middle cerebral artery occlusion in rats. *Exp Neurol*. 2001;169:56–63.
28. Kawashima S, Yamashita T, Miwa Y, Ozaki M, Namiki M, Hirase T, Inoue N, Hirata K, Yokoyama M. HMG-CoA reductase inhibitor has protective effects against stroke events in stroke-prone spontaneously hypertensive rats. *Stroke*. 2003;34:157–163.
29. Sumi D, Hayashi T, Thakur NK, Jayachandran M, Asai Y, Kano H, Matsui H, Iguchi A. A HMG-CoA reductase inhibitor possesses a potent anti-atherosclerotic effect other than serum lipid lowering effects–the relevance of endothelial nitric oxide synthase and superoxide anion scavenging action. *Atherosclerosis*. 2001;155:347–357.
30. Morita H, Saito Y, Ohashi N, Yoshikawa M, Katoh M, Ashida T, Kurihara H, Nakamura T, Kurabayashi M, Nagai R. Fluvastatin ameliorates the hyperhomocysteinemia-induced endothelial dysfunction: The antioxidative properties of fluvastatin. *Circ J*. 2005;69:475–480.
31. Endres M. Statins and stroke. *J Cereb Blood Flow Metab*. 2005;25:1093–1110.

Table I. Statistics in Morris Water Maze

	Hidden Test			Visible Test		
	Latency	Length	Speed	Latency	Length	Speed
P values in 2-factor repeated-measure ANOVA (Sham, MCAo+S, MCAo+F)						
Treatment	<0.001	<0.001	0.053	0.004	0.021	0.342
Day	<0.001	0.011	<0.001	0.003	0.014	0.288
Treatment×Day	0.002	<0.001	0.855	0.465	0.684	0.306
P values in Scheffe test on day 4						
Sham vs MCAo+S	<0.001	<0.001	0.933	0.018	0.025	0.585
Sham vs MCAo+F	0.024	0.010	0.277	0.138	0.058	0.266
MCAo+S vs MCAo+F	0.012	0.023	0.129	0.643	0.941	0.820

MCAo+S indicates saline-treated rats after MCAo; MCAo+F, fluvastatin-treated rats after MCAo.

ORIGINAL ARTICLE ACTA RADIOLOGICA

Comparison of Gd-DTPA-Induced Signal Enhancements in Rat Brain C6 Glioma among Different Pulse Sequences in 3-Tesla Magnetic Resonance Imaging

H. SATO, J. ENMI, N. TERAMOTO, T. HAYASHI, A. YAMAMOTO, T. TSUJI, H. NAITO & H. IIDA

Laboratory for Diagnostic Solutions and Department of Investigative Radiology, Advanced Medical Engineering Center, Research Institute, National Cardiovascular Center, Osaka, Japan; Diagnostic Imaging Medical Affairs, Medical Affairs, Product Development Department, Bayer Yakuhin, Ltd., Osaka, Japan; Department of Radiology, Hospital of National Cardiovascular Center, Osaka, Japan

Sato H, Enmi J, Teramoto N, Hayashi T, Yamamoto A, Tsuji T, Naito H, Iida H. Comparison of gd-dtpa-induced signal enhancements in rat brain c6 glioma among different pulse sequences in 3-tesla magnetic resonance imaging. Acta Radiol 2007;000:1–8.

Background: T1-shortening contrast media are routinely used in magnetic resonance (MR) examinations for the diagnosis of brain tumors. Although some studies show a benefit of 3 Tesla (T) compared to 1.5T in delineation of brain tumors using contrast media, it is unclear which pulse sequences are optimal.

Purpose: To compare gadopentetate dimeglumine (Gd-DTPA)-induced signal enhancements in rat brain C6 glioma in the thalamus region among different pulse sequences in 3T MR imaging.

Material and Methods: Five rats with a surgically implanted C6 glioma in their thalamus were examined. T1-weighted brain images of the five rats were acquired before and after Gd-DTPA administration (0.1 mmol/kg) using three clinically available pulse sequences (spin echo [SE], fast SE [FSE], fast spoiled gradient echo [FSPGR]) at 3T. Signal enhancement in the glioma (E_T) was calculated as the signal intensity after Gd-DTPA administration scaled by that before administration. Pulse sequences were compared using the Tukey-Kramer test.

Results: E_T was 1.12 ± 0.05 for FSE, 1.26 ± 0.11 for FSPGR, and 1.20 ± 0.11 for SE. FSPGR showed significantly higher signal enhancement than FSE and comparable enhancement to SE.

Conclusion: FSPGR is superior to FSE and comparable to SE in its ability to delineate rat brain C6 glioma in the thalamus region.

Key words: Brain; contrast agents; MR imaging

Hiroshi Sato, Laboratory for Diagnostic Solutions, Advanced Medical Engineering Center, Research Institute, National Cardiovascular Center, 5-7-1 Fujishiro-dai, Suita, Osaka 565-8565, Japan (fax. +81 6 6835 5429, e-mail. camo@ri.ncvc.go.jp)

Accepted for publication August 5, 2007

T1-shortening contrast media are routinely used in magnetic resonance (MR) examinations for the diagnosis of brain tumors. Some studies show a benefit of 3 Tesla (T) compared to 1.5T in delineation of brain tumors using contrast media (1–5). However, it is unclear which pulse sequences are optimal. The conventional spin-echo (SE) technique has been most frequently used for T1-weighted (T1W) imaging of tumors after contrast media administration. The gradient-echo (GRE) technique, which is faster than SE, was introduced initially at 1.5T or lower field strength (6–11). Some studies have reported that GRE techniques compare favorably with the SE technique for delineation of brain tumors (8–10), while other studies have reported that GRE techniques do not show contrast enhancement as well as SE (6, 7, 11). At 3T, as at 1.5T or lower field strength, the issue of whether GRE techniques are effective compared to SE has not been determined. In 16 patients, NÖBAUER-HUMANN et al. reported that 3D GRE with magnetization preparation (MPRAGE) was comparable to T1W SE in tumor-to-brain contrast at 3T, although the parameters of T1W SE were not

informa
healthcare

DOI 10.1080/02841850701630326

optimized for 3T (1). In 12 patients, FISCHBACH et al. compared four T1W sequences: SE, inversion recovery fast SE (IR-FSE), 2D GRE, and MPRAGE at 3T. They observed that SE and IR-FSE provided higher contrast enhancement of brain tumors than 2D GRE and MPRAGE. Furthermore, their impressions showed that the visual quality of SE was superior to that of the other three sequences (12).

In order to compare pulse sequences, it would be preferable if the pathological and physiological conditions of subjects were constant across scans. One possible model system is the widely used rat brain glioma model (4, 5, 13–15). In most studies with small animals, MR imaging systems with small magnets are widely used. The pulse sequences available on the scanner designed for small animals, however, are different from those on a clinical scanner. By using a scanner designed for humans, we can compare diagnostic values of practical clinical pulse sequences. To our knowledge, no studies have been reported comparing pulse sequences on a 3T human scanner using a rat brain glioma model.

The purpose of the current study was to elucidate the optimal pulse sequence that provides the highest obtainable signal enhancement using gadopentetate dimeglumine (Gd-DTPA) in a rat brain C6 glioma model on a 3T human whole-body scanner.

Material and Methods

Protocols of all animal procedures were approved by the ethics committee for animal research at the National Cardiovascular Center. Male Sprague-Dawley rats (Japan SLC, Inc., Shizuoka, Japan) were used. Rats had free access to food and water, and were kept in uncrowded conditions (two/cage) in a light-, temperature-, and humidity-regulated room (light on 07.00–19.00, 23 ± 3°C, and 50 ± 20%).

Study design

T1 measurements in the brains of three normal rats and phantom studies were performed to identify pulse sequences, among which Gd-DTPA-induced signal enhancements in rat C6 brain gliomas were compared, and to determine pulse sequence parameters. Using the determined pulse sequences and parameters, we examined five rats with developed gliomas out of 20 rats that received C6 glioma implantation in their thalamus region.

MR imaging system

All scanning was performed on a 3T whole-body scanner (Signa LX VH3M4; GE Healthcare, Milwaukee, Wisc., USA) equipped with the manufacturer's gradient system (maximum gradient strength 40 mT/m; slew rate 150 mT/m/s).

For imaging rat brains, we built a three-turn solenoid coil with a diameter of 42 mm and a length along the cylindrical axis of 18 mm. The diameter and length of this coil were adjusted to rat head size. The helical pitch of the coil was wide enough to pass the ear bars used to secure the rat's head. The coil was capable of transmission and reception, and was tuned to an impedance of 50 Ω at a resonant frequency of 127.76 MHz. Capacitance was divided into six elements in series, which were put at each half turn. The coil was mounted on a fixing apparatus (Narishige Co., Ltd., Tokyo, Japan) using an acrylic jig specially designed for the coil (Fig. 1). Rats were placed prone on the fixing apparatus. Rat heads were secured using an incisor hook and ear bars. All components of the fixing apparatus consisted of non-magnetic materials. During imaging, the fixing apparatus, on which the rat and the coil were mounted, was placed in the gantry so that the cylindrical axis of the coil and the cranial-to-caudal direction of the rat were perpendicular to a static magnetic field, and the center of the rat brain was positioned at the magnet isocenter.

Measurement of T1 in normal rat brain

This measurement was performed to establish the normal T1 value in the transplantation site (thalamus) of the C6 glioma cells. T1 values in the brain of three normal rats (9–13 weeks old, 380 ± 50 g) were

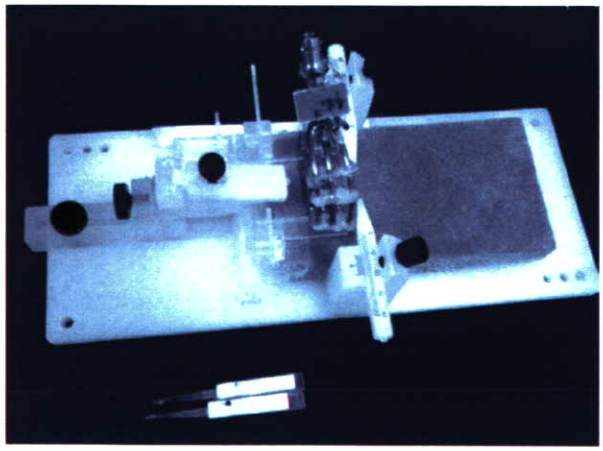

Fig. 1. The three-turn solenoid coil and the fixing apparatus used for the imaging of rats in the present study. The coil was mounted on the fixing apparatus using the specially designed acrylic jig.

Acta Radiologica rad134548.3d 23/10/07 20:33:23
The Charlesworth Group, Wakefield +44(0)1924 369598 - Rev 7.51n/W (Jan 20 2003)
262880

measured by using a saturation recovery method with a variable repetition time (TR) SE imaging sequence (16): TR 600, 1000, 2000, 4000, 8000 ms; echo time (TE) 10 ms; bandwidth (BW) 16 kHz; field of view (FOV) 40 × 30 mm; matrix size 256 × 160; slice thickness 1 mm; slice gap 1 mm; number of slices 16; number of excitations (NEX) 1; coronal plane. An 8-cm polyvinyl chloride tube with an outer diameter of 2.7 mm was inserted into the animal's trachea, and the rats were ventilated with an average of 2–3 ml per breath of a mixture of O_2, N_2, and air (2:1:10) using a small animal ventilator (CWE SAR-830/AP Ventilator; CWE, Inc., Ardmore, Pa., USA) at an average of 80 breaths per minute. Body temperature was monitored rectally (36.0 ± 0.5°C).

T1 values were estimated on a pixel-by-pixel basis using the non-linear least-square fit of the signal intensity measured for each TR value. In the obtained T1 images, regions of interest (ROIs) were placed on the thalamus, hippocampus, olfactory bulb, cerebral cortex, corpus callosum, midbrain, cerebellum, pons, cerebrospinal fluid, and muscle. Mean T1 values were calculated from each ROI. A mean and a standard deviation of the mean values obtained from three rats were calculated.

Phantom study

Phantom preparation. Gd-DTPA (Magnevist; Bayer Schering Pharma, Osaka, Japan) was diluted with saline to obtain 19 solutions with different concentrations (0, 0.01, 0.03, 0.05, 0.07, 0.1, 0.15, 0.2, 0.25, 0.3, 0.5, 0.7, 1, 3, 5, 7, 10, 30, and 50 mM). Each solution was encapsulated in separate polypropylene vials with a diameter of 27 mm, which were set in agar.

T1 measurement. T1 values of each Gd-DTPA solution were measured at room temperature using the same pulse sequence as the T1 measurement in normal rats: TR 34, 100, 200, 400, 600, 800, 1000, 1200, 1400, 1600, 1800, 2000, 4000, 6000, 8000, 11,000, 15,000 ms; TE 9 ms; BW 16 kHz; FOV 210 × 158 mm; matrix size 256 × 192; slice thickness 3 mm; number of slices 1; NEX 1. A standard quadrature birdcage head coil was used.

Circular ROIs with 70–80% of the diameter of a vial were placed on a homogeneous signal portion of each phantom image. T1 values were estimated by non-linear least-square fit of the average signal intensity of all voxels in the ROI measured for each TR value. Five measurements were performed for phantoms, and the mean and standard deviation of measured T1 values were calculated.

Choice of pulse sequences. We used a Gd-DTPA saline solution (0.1 mM) with a T1 value close to that in the normal thalamus as a corresponding solution to the glioma in the thalamus region before contrast. We hypothesized that T1 in the glioma would not be so different from that in normal tissue. Saline solutions with a higher concentration of Gd-DTPA were regarded as a corresponding solution to the glioma after contrast.

T1W images of each phantom were acquired at room temperature (approximately 21°C) using four clinically available pulse sequences (SE, fast SE [FSE], IR-FSE [T1FLAIR], and fast spoiled GRE [FSPGR]) (Table 1). A standard quadrature birdcage head coil was used for the imaging of phantoms.

Circular ROIs with 70–80% of the diameter of the vial were placed on a uniform signal portion of each phantom. Mean signal intensities were calculated from each ROI. For each sequence, signal enhancements of each Gd-DTPA solution (E_P) were calculated as $E_P = S/S_0$, where S is the signal intensity of each solution and S_0 is that of 0.1 mM of the solution. The pulse sequences showing high E_P were used for the imaging of C6 glioma model rats and were compared based on Gd-DTPA-induced signal enhancements in brain tumors, delineated by histopathology.

Rat brain C6 glioma model study

Preparation of rat brain C6 glioma models. C6 glioma cells (CCL-107 cell line, ATCC; Summit Pharmaceuticals International Corporation, Tokyo,

Table 1. Pulse sequences and imaging parameters used for imaging of saline phantoms containing gadopentetate dimeglumine (Gd-DTPA)

Pulse sequence	TR, ms	TE, ms	TI, ms	FA, °	ETL	BW, kHz	NEX	Acquisition time, min:s
SE	1400	14	—	—	—	16	1	4:46
FSE	1400	16	—	—	3	32	1	1:52
T1FLAIR	3000	16	1300	—	3	32	1	4:00
FSPGR	20	3.2	—	30	—	32	10	0:39

For all pulse sequences, FOV was 210 × 158 mm, matrix was 256 × 192, the number of slices was 1, and the slice thickness was 3 mm. SE: spin echo; FSE: fast spin echo; T1FLAIR: inversion recovery fast spin echo; FSPGR: fast spoiled gradient echo; TR: repetition time; TE: echo time; TI: inversion time; FA: flip angle; ETL: echo train length; BW: bandwidth; NEX: number of excitations.

Japan) were implanted into the region of the thalamus in the left hemispheres of the brains of 20 rats (8 weeks old, 292.8 ± 14.8 g). The implantation procedures were performed under general anesthesia using an intramuscular injection of ketamine (33 mg/kg; Sankyo Co., Ltd., Tokyo, Japan) and xylazine (7 mg/kg; Bayer AG, Leverkusen, Germany). A burr hole was made 3 mm lateral and 2 mm posterior to the bregma using a dental drill. A needle with an outer diameter of 0.3 mm was inserted 4 mm below the outer table of the skull through the burr hole. A 10-μl solution containing 10^7 cells/ml was infused over 5 min at a constant rate using a microsyringe (Hamilton Co., Reno, Nev., USA) and infusion pump (Eicom Corp., Kyoto, Japan).

MR imaging. Two weeks after implantation, all 20 rats underwent screening by T1W imaging after Gd-DTPA administration. Developed glioma was confirmed in only five out of 20 rats. Those five rats were used for experiments for the comparison of pulse sequences. Three weeks after implantation, when the glioma was fully developed, T1W brain images of the selected five rats (11 weeks old, 301.3 ± 29.0 g) were acquired before and after Gd-DTPA administration using three pulse sequences determined by the phantom study (Table 2) in the coronal plane. Rats were given general anesthesia with an intramuscular injection of a ketamine (33 mg/kg) and xylazine (7 mg/kg) mixture, and allowed to breathe spontaneously during preparation and imaging. First, precontrast T1W images were acquired. Then, a dose of 0.1 mmol/kg of Gd-DTPA was administered by hand injection followed by a 3.0-ml saline flush through a 22G indwelling needle placed in a tail or femoral vein. Postcontrast T1W imaging started 1 min after Gd-DTPA administration with identical settings to the precontrast imaging. Each rat was examined using all three pulse sequences (Table 2). In order to eliminate the effect of previously administered Gd-DTPA, three scans using different pulse sequences were performed on three separate days, at 22- to 26-hour intervals, in a randomized order.

ROI analysis. Based on the results of histopathology (see below), ROIs were placed on a portion of each glioma. Areas of necrosis or hemorrhage were excluded from the ROI. Mean signal intensities in the pre- and postcontrast T1W images were calculated from each ROI. For each sequence, signal enhancement of each glioma (E_T) was calculated as $E_T = S_{post}/S_{pre}$, where S_{post} is signal intensity in the glioma after contrast and S_{pre} is that before contrast.

Histopathology

One day after MR imaging, rat brains were removed and fixed in formalin. All brains were completely coronally sectioned. Sections were stained with hematoxylin and eosin (HE) in order to delineate areas of glioma, hemorrhage, and necrosis.

Statistical analysis

All parameters assessed were given as means ± standard deviations. Pair-wise comparison among pulse sequences was performed using the Tukey-Kramer test. A P value of <0.05 was considered statistically significant.

Results

T1 in normal rat brains

Fig. 2 shows images from one of the three normal rats used to quantitate T1 values in the brain. Table 3 summarizes the T1 values of typical brain structures. The T1 value in the thalamus was 1405 ± 32 ms.

T1 of Gd-DTPA solutions

Fig. 3 shows selected images from a series of 17 images obtained with different TR values. Table 4 summarizes T1 values in the Gd-DTPA solutions

Table 2. Pulse sequences and imaging parameters used for imaging of rat brains with C6 glioma cell implants

Pulse sequence	TR, ms	TE, ms	FA, °	ETL	BW, kHz	NEX	Acquisition time, min:s
SE	1400	13	—	—	16	1	4:46
FSE	1400	18.6	—	3	32	3	4:32
FSPGR	20	4.7	30	—	32	8	5:40

For all pulse sequences. FOV was 60 × 45 mm, matrix was 256 × 192, the number of slices was 11, and the slice thickness was 2.5 mm (0.5-mm gap). SE: spin echo; FSE: fast spin echo; FSPGR: fast spoiled gradient echo; TR: repetition time; TE: echo time; FA: flip angle; ETL: echo train length; BW: bandwidth; NEX: number of excitations.

Acta Radiologica rad134548.3d 23/10/07 20:33:24
The Charlesworth Group, Wakefield +44(0)1924 369598 - Rev 7.51n/W (Jan 20 2003)
262880

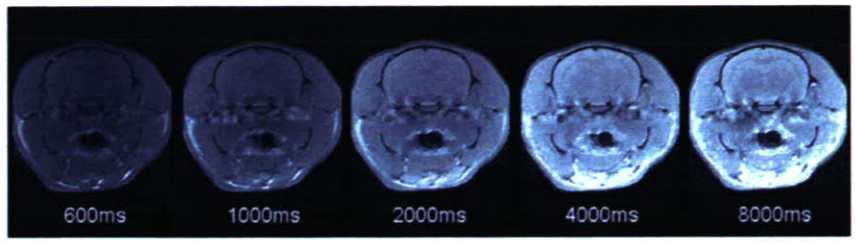

Fig. 2. Images from one of three rats used for the measurement of T1 values in normal rat brain. One of 16 slices acquired is shown. The images are arranged from left to right in ascending order of repetition time. All five images are set with equal window width and equal window level.

Table 3. T1 relaxation time in normal rat brain at 3T

	T1, ms
Thalamus	1405 ± 32
Hippocampus	1779 ± 151
Olfactory bulb	1613 ± 117
Cerebral cortex	1506 ± 13
Corpus callosum	1389 ± 43
Midbrain	1329 ± 50
Cerebellum	1726 ± 356
Pons	1343 ± 80
Cerebrospinal fluid	3460 ± 737
Muscle	1529 ± 99

Mean and standard deviation of values obtained from three rats.

ranging from 0 to 10 mM. In 30 and 50 mM solutions, an accurate T1 value could not be measured because of extensive signal loss due to T2 decay. The 0.1-mM solution showed a T1 value (1302 ± 54 ms) closest to that in the normal thalamus (1405 ± 32 ms).

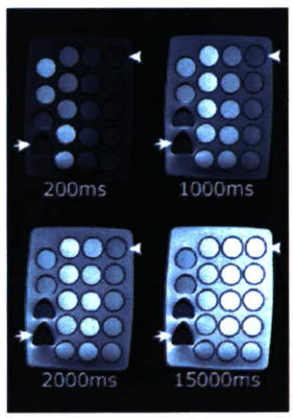

Fig. 3. Images obtained in the measurement of T1 values of 19 saline solutions with different concentrations of gadopentetate dimeglumine (0, 0.01, 0.03, 0.05, 0.07, 0.1, 0.15, 0.2, 0.25, 0.3, 0.5, 0.7, 1, 3, 5, 7, 10, 30, and 50 mM). The four selected images from a series of 17 images obtained with different TR values are shown. Each solution was encapsulated in separate polypropylene vials, which were set in agar. The concentration of gadopentetate dimeglumine decreases from bottom to top and from left to right. Arrows and arrowheads denote the 50-mM and 0-mM solutions, respectively. All four images are set with equal window width and equal window level.

Table 4. T1 of saline with different concentrations of Gd-DTPA at 3T

Gd-DTPA concentration, mM	T1, ms
0	3026 ± 121
0.01	2652 ± 96
0.03	2245 ± 108
0.05	1970 ± 92
0.07	1775 ± 103
0.1	1302 ± 54
0.15	993 ± 57
0.2	820 ± 52
0.25	737 ± 51
0.3	666 ± 63
0.5	389 ± 17
0.7	284 ± 12
1	209 ± 9
3	84 ± 4
5	58 ± 2
7	36 ± 1
10	27 ± 1
30	—
50	—

Mean and standard deviation of values obtained from five measurements.

Choice of pulse sequences

Fig. 4 shows E_P in the Gd-DTPA solutions ranging from 0.1 to 50 mM. In Gd-DTPA solutions ranging from 0.15 to 30 mM, a higher E_P was obtained as follows: FSPGR > SE > FSE > T1FLAIR. Because E_P for T1FLAIR was lowest at all concentrations, T1FLAIR was not used for the imaging of rat brain tumors.

Based on our preliminary experiments, the T1 value in the glioma in the thalamus region after contrast was about 90% of that before contrast. Therefore, we regarded the 0.15-mM solution as a corresponding solution to glioma after contrast, and compared E_P values at 0.15 mM obtained using different sequences (Fig. 5). E_P at 0.15 mM was 1.10 ± 0.02 for FSE, 1.16 ± 0.01 for FSPGR, 1.16 ± 0.01 for SE, and 1.06 ± 0.01 for T1FLAIR. The Tukey-Kramer test showed significant differences ($P < 0.05$) between all pairs except for FSPGR–SE. E_P for FSPGR was significantly higher than that for FSE and T1FLAIR and comparable to that for SE.

Acta Radiologica **rad134548.3d** 23/10/07 20:33:24
The Charlesworth Group, Wakefield +44(0)1924 369598 - Rev 7.51n/W (Jan 20 2003)
262880

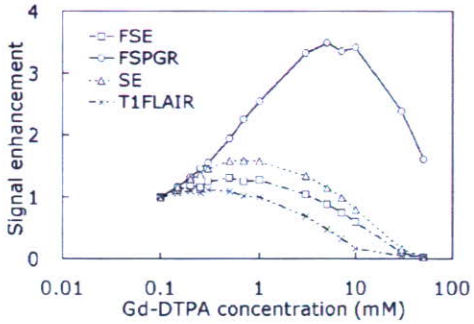

Fig. 4. Signal enhancements in saline solutions containing gadopentetate dimeglumine (Gd-DTPA) obtained by the following pulse sequences: spin echo (SE); fast spin echo (FSE); inversion recovery fast spin echo (T1FLAIR); fast spoiled gradient echo (FSPGR). Signal enhancement was the signal intensity scaled by that of a 0.1-mM Gd-DTPA solution whose T1 value was closest to the average T1 value in the brain parenchyma of normal rats.

Signal enhancement in rat brain C6 glioma

Fig. 6 displays typical pre- and postcontrast T1W images of brains of C6 glioma model rats, together with an example of ROIs placed on the glioma and HE-stained slices. Fig. 7 shows the comparison between E_T values for FSE, SE, and FSPGR. E_T values were 1.12 ± 0.05 for FSE, 1.26 ± 0.11 for FSPGR, and 1.20 ± 0.11 for SE. The Tukey-Kramer test showed the significant superiority of FSPGR over FSE. There was no significant difference between FSPGR and SE.

Discussion

T1W imaging using SE results in a corresponding restriction in the number of slices as a result of the

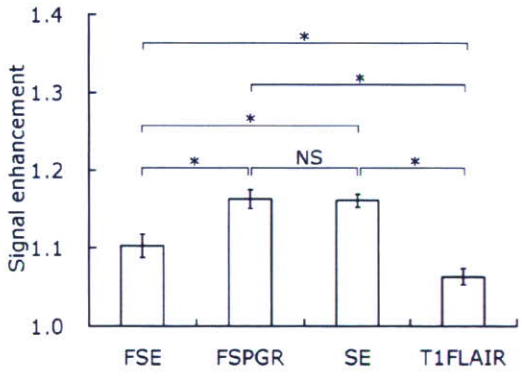

Fig. 5. Signal enhancement of saline solution with 0.15 mM Gd-DTPA obtained using different pulse sequences: spin echo (SE); fast spin echo (FSE); inversion recovery fast spin echo (T1FLAIR); fast spoiled gradient echo (FSPGR). Signal enhancement was defined as the signal intensity of a 0.15-mM solution scaled by that of a 0.1-mM solution. The Tukey-Kramer test was performed for pair-wise comparison among four pulse sequences. The asterisk and NS denote significant difference ($P<0.05$) and no significant difference ($P>0.05$), respectively.

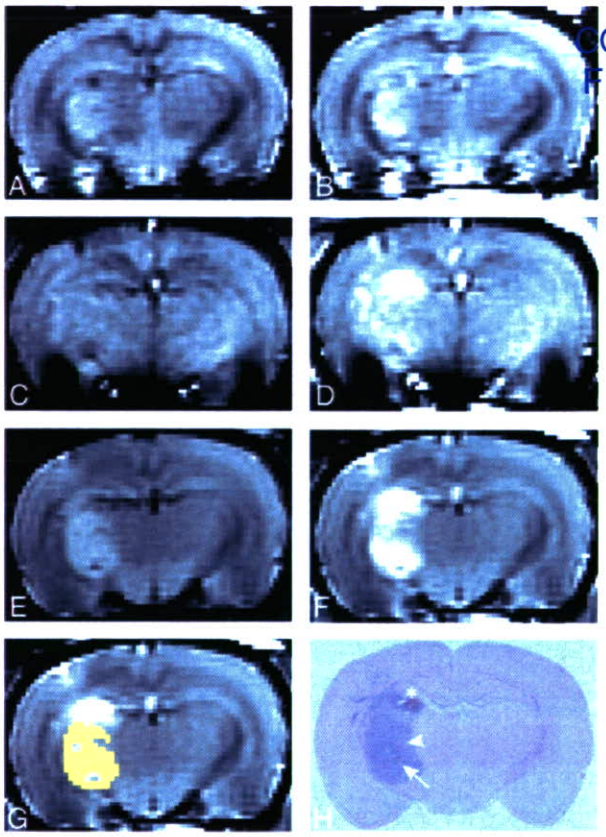

Fig. 6. Examples of pre- (A, C, E) and post-contrast (B, D, F) coronal T1-weighted images obtained using fast spin-echo (FSE) (A, B), fast spoiled gradient-echo (FSPGR) (C, D), and spin-echo (SE) (E, F) sequences. A region of interest (ROI) placed on the glioma (G) and a slice stained using hematoxylin and eosin (HE) (H). T1-weighted images were acquired 3 weeks after the implantation of C6 glioma cells. Areas of necrosis or hemorrhage, which were delineated based on histopathology, were excluded from ROIs. In the HE-stained slice, small-cell glioma (arrowhead), hemorrhage (asterisk), and necrosis (arrow) were found.

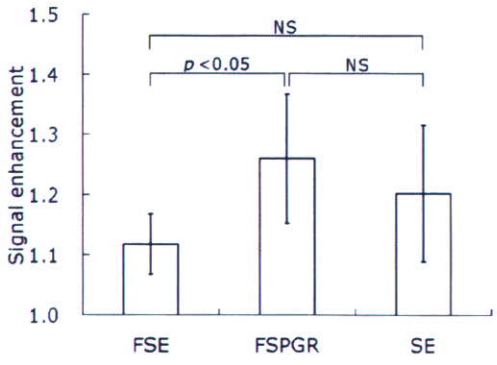

Fig. 7. Signal enhancement in rat brain C6 glioma obtained with different pulse sequences: spin echo (SE); fast spin echo (FSE); fast spoiled gradient echo (FSPGR). Signal enhancement was defined as the signal intensity after Gd-DTPA administration scaled by that before administration. The pair-wise comparison among pulse sequences was performed using the Tukey-Kramer test. NS denotes no significant difference ($P>0.05$).

specific absorption rate (SAR) at 3T. The use of FSE makes radiofrequency heating more serious. Compared to SE and FSE, FSPGR provides relatively low radiofrequency heating and, if the NEX of FSPGR can be reduced, relatively short acquisition time. This depends on the signal-to-noise ratio, and we thought it possible based on our rat brain images (Fig. 6). Therefore, we examined the characteristics of signal enhancement in FSPGR. FSPGR provided significantly higher signal enhancement than FSE and comparable signal enhancement to SE, both in the 0.15-mM Gd-DTPA solution and in rat brain C6 glioma in the thalamus region. We speculate that FSPGR may be superior to FSE and comparable to SE in its ability to delineate brain tumors, although, in order to verify this speculation, several studies would be required using different cell types and various transplantation sites. Considering the advantage of FSPGR in terms of acquisition time and SAR limit, FSPGR may be more suitable for contrast-enhanced T1W imaging of brain tumors in clinical 3T scanners than SE. Additionally, high-resolution 3D images can be obtained by using FSPGR with a reasonable acquisition time so that small lesions may be better visualized. On the other hand, FSPGR was more sensitive to magnetic susceptibility artifacts than SE (Fig. 6). SE could therefore be more suitable than FSPGR for delineation of tumors in regions with susceptibility artifacts, such as the base of the skull.

E_T values obtained in our study (1.26 for FSPGR, 1.20 for SE, and 1.12 for FSE) were lower compared to previously reported values (1, 4, 5, 12). For example, RUNGE et al. reported that the E_T induced by Gd-DTPA was approximately 1.44 using SE in rat brain C6/LacZ glioma models at 3T (5). The difference between E_T in our study and that in previous reports may result from the difference in the type of tumor, in the degree of growth of brain tumors, or in TR. In our study, TR was adjusted to increase T1 contrast in the normal brain region for specification of more exact location of the glioma. Although the use of a shorter TR may increase signal enhancement in the glioma, contrast in the normal region would become unclear, and therefore it could become difficult to specify the location of the glioma exactly. Therefore, we used a longer TR than that in previous reports.

FISCHBACH et al. showed higher contrast in SE in patients, but they optimized the TR (600 ms) of SE by phantom experiments using a saline solution with a low concentration of Gd-DTPA (0.125 μM) (12), whose T1 is extremely long compared to that in the brain. We quantified T1 in rat brains and chose a proper TR (1400 ms) of SE to enhance normal brain contrast. Therefore, our comparison would be fairer and our results may be more closely extrapolated to human tumors.

One limitation of our work is our limited sample size. Although C6 glioma cells were implanted into 20 rats in our in-vivo study, only five rats could be used for the experiment, as C6 gliomas showed considerable individual variation in their growth and were fully developed only in five rats. Therefore, the number of test animals was relatively small, resulting in large standard deviations for E_T. A larger sample size may show a significant difference between FSPGR and SE.

In conclusion, FSPGR is superior to FSE and comparable to SE in its ability to delineate rat brain C6 glioma in the thalamus region using venous injection of Gd-DTPA.

Acknowledgments

This study was supported by a research grant on Advanced Medical Technology from the Ministry of Health, Labor and Welfare (MHLW), Japan (H17-nano-15), and a Program for Promotion of Fundamental Studies in Health Science of the Organization for Pharmaceutical Safety and Research (of Japan) Health Science Research Grant (H13-005) from the Ministry of Health, Labor and Welfare, (of Japan)

References

1. Nöbauer-Huhmann IM, Ba-Ssalamah A, Mlynarik V, Barth M, Schoggl A, Heimberger K, et al. Magnetic resonance imaging contrast enhancement of brain tumors at 3 tesla versus 1.5 tesla. Invest Radiol 2002;37:114–9.
2. Trattnig S, Ba-Ssalamah A, Noebauer-Huhmann IM, Barth M, Wolfsberger S, Pinker K, et al. MR contrast agent at high-field MRI (3 Tesla). Top Magn Reson Imaging 2003;14:365–75.
3. Ba-Ssalamah A, Nöbauer-Huhmann IM, Pinker K, Schibany N, Prokesch R, Mehrain S, et al. Effect of contrast dose and field strength in the magnetic resonance detection of brain metastases. Invest Radiol 2003;38:415–22.
4. Biswas J, Nelson CB, Runge VM, Wintersperger BJ, Baumann SS, Jackson CB, et al. Brain tumor enhancement in magnetic resonance imaging: comparison of signal-to-noise ratio (SNR) and contrast-to-noise ratio (CNR) at 1.5 versus 3 tesla. Invest Radiol 2005;40: 792–7.
5. Runge VM, Biswas J, Wintersperger BJ, Baumann SS, Jackson CB, Herborn CU, et al. The efficacy of gadobenate dimeglumine (Gd-BOPTA) at 3 Tesla in brain magnetic resonance imaging: comparison to 1.5